Eur. Phys. J. E **6**, 287–294 (2001)

THE EUROPEAN PHYSICAL JOURNAL E

EDP Sciences

Structure and frustration in liquid crystalline polyacrylates II. Thin-film properties

B.I. Ostrovskii[1,2], D. Sentenac[1], I.I. Samoilenko[2], and W.H. de Jeu[1,a]

[1] FOM-Institute for Atomic and Molecular Physics, Kruislaan 407, 1098 SJ Amsterdam, The Netherlands
[2] Institute of Crystallography, Academy of Sciences of Russia, Leninsky pr. 59, Moscow, 117333 Russia

Received 28 February 2001 and Received in final form 6 August 2001

Abstract. We report on the thin-film behaviour of a polyacrylate with phenyl benzoate mesogenic side groups and a narrow polydispersity. Depending on the degree of polymerisation, these polymers show a nematic, a smectic-A_d, a re-entrant nematic and a $\tilde{C}$ phase with a two-dimensional monoclinic lattice. X-ray reflectivity and atomic-force microscopy have been used to characterize the structure and surface morphology. The system exhibits two stable side-chain packing configurations with incommensurate spacings that can be both stabilized at a free surface. Thin films in the nematic phase show a structural dewetting induced by the growth of surface domains of the $\tilde{C}$ phase. Additionally, surface-induced ripples with a nanoscale lateral period form at the air-film interface. We attribute these patterns to a coupling between the local liquid crystalline ordering of the mesogenic side groups and the surface curvature energy.

PACS. 64.70.Md Transitions in liquid crystals – 78.70.Ck X-ray scattering – 61.30.Eb Experimental determinations of smectic, nematic, cholesteric, and other structures

1 Introduction

In the preceding paper [1] (hereafter referred to as I) we discuss the bulk behaviour of a new frustrated side-chain liquid crystalline (LC) polyacrylate system (PABB-5). These polymers show at low degree of polymerisation P_w a nematic (N) phase. Upon increasing P_w above the re-entrant point $P_w(\mathrm{RP}) = 42$, a smectic A_d (Sm-A_d) phase appears, which becomes unstable with decreasing temperature and melts into a re-entrant nematic (RN) phase. In all cases upon further cooling a $\tilde{C}$ phase is formed which has a two-dimensional (2D) monoclinic lattice (see Fig. 1 of I). As expected, the layers in the Sm-A_d phase are formed by partially overlapping side groups, giving a periodicity incommensurate with the length of a mesogenic unit. The $\tilde{C}$ phase consists of a 2D oblique lattice of side chains, which are arranged in chevron-like blocks of "almost bilayers". Liquid-like order is retained in the third dimension. Evidently two competing length scales are present in the system. The first one is about 3.5 nm and can condense into a Sm-A_d phase. This type of layering is stable at high temperatures and for relatively long polymer chains. The second length is about 4.4 nm and can exist only on a local scale. It leads to the formation of a highly defective $\tilde{C}$ phase. This type of ordering is stable at relatively low temperatures and exists for a broad range of P_w values starting from oligomers. However, the 4.4 nm length exerts its influence even far away from the N-$\tilde{C}$ and RN-$\tilde{C}$ transition lines, and dominates over the whole region of the phase diagram for $P_w < P_w(\mathrm{RP})$. It seems that the frustrated behaviour in PABB-5 is driven by changes of the polymer backbone conformation, which become more pronounced for long chains. The existence of two competing length scales at almost equal free energies makes the series unique, and consequently a strong sensitivity to external stimuli can be expected.

In this paper we present a structural study of films of PABB-5 on a substrate using a combination of X-ray reflectometry (XR) and atomic force microscopy (AFM). XR is sensitive to the electron density modulations along the film normal and provides information about any layering in the film and at the interfaces. AFM studies give complementary information about the surface topography. The free surface is found to stabilise the incommensurate spacings existing in the system. A structural dewetting has been observed in the N and RN phases, which is induced by the growth of surface domains with a local $\tilde{C}$ structure. Additionally, surface-induced ripples with a ~ 9 nm lateral period and a sub-nanometer height modulation are observed at the air-film interface [2]. In the area of self-organized surface structures [3–6] they present a new type of pattern realized on a homogeneous substrate. We propose an explanation in terms of a locally frustrated layering of the LC side groups that couples to the surface curvature.

[a] e-mail: dejeu@amolf.nl

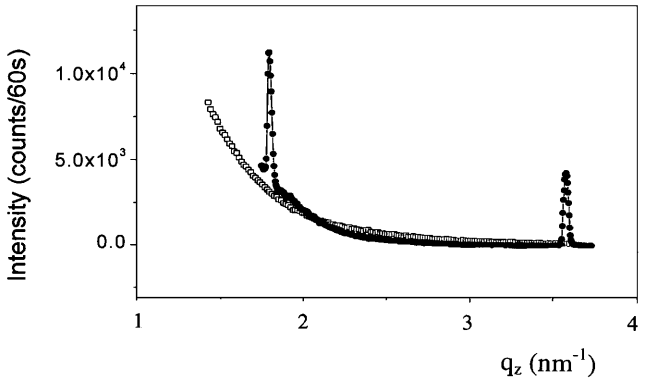

Fig. 1. X-ray intensity profiles as a function of q_z for a 10 μm thick film with $P_w = 55$ in the Sm-A_d phase. Open squares: annealed at $T = 115\,^\circ$C; filled dots: annealed at $T = 93\,^\circ$C.

2 Experimental

The LC polyacrylates with phenyl benzoate mesogenic groups (see Fig. 1 of I) were synthesized and fractionated into highly monodisperse samples as described in [7]. The polydispersity was as small as $\overline{M}_w/\overline{M}_n \approx 1.1$. The various phases were identified by their characteristic X-ray diffraction features. Investigations were made for $P_w = 37$ (phase transitions in °C: glass 41 $\tilde{C}$ 55 N 126 isotropic) and $P_w = 55$ (phase transitions: glass 41 $\tilde{C}$ 59 RN 91 Sm-A_d 125 N 133 isotropic). Films with a thickness ranging from 20 to 90 nm were prepared by spin-coating from toluene solutions onto float glass substrates. The film thickness was tuned by changing the spinning velocity (1500–3000 rpm) and the polymer concentration (6–14 mg/mL). Some relatively thick uniform films (μm range) were made by a spreading technique similar as used for drawing freely suspended smectic films [8]. All films were annealed for 10–16 hours in the Sm-A_d or N phase at $T = 90$–$100\,^\circ$C in a dry nitrogen atmosphere. For the XR measurements the samples were placed in a two-stage oven providing temperature stability within 0.1 °C. At each temperature the sample was equilibrated for 3–6 hours, which removed any hysteresis upon changing the temperature. For the AFM investigations the samples were quenched to room temperature into their glassy state.

XR was performed with the triple-axis diffractometer described in I. Direct images of the polymer film surface were obtained with an AFM (Solver SFM, NT-MDT, Zelenograd, Moscow) in the semi-contact (tapping) mode. Standard probes with a tip radius of about 10 nm were used at a cantilever resonant frequency of approximately 300 kHz.

3 Results

To get preliminary information about PABB-5 film properties, Figure 1 shows XR data from a 10 μm film annealed in the Sm-A_d phase at $T = 115\,^\circ$C. In reciprocal space, the specular scans probe the scattered intensity along q_z perpendicular to the film. A general decay of the intensity is observed corresponding to the Fresnel reflectivity from the rough surface, while there is no indication of any Bragg peak. On cooling down to about $T = 93\,^\circ$C drastic changes occur in the specular reflectivity and two orders of resolution-limited Bragg peaks are observed. The associated periodicity of 3.53 nm corresponds closely to the bulk Sm-A_d spacing. This implies that the smectic layers are parallel to the surface, with the mesogenic side groups anchoring homeotropically. The mosaicity, determined by a transverse scan (rocking scan) across the specular reflectivity, was typically about 0.03°(FWHM). This ordering transformation occurs in a narrow temperature range 91–95 °C in the vicinity of the Sm-A_d–RN phase transition line, and is reversible upon cycling the temperature. The complete smectic layer rearrangement takes about 2-3 hours, as determined by monitoring the Bragg-peak intensity. On cooling down from the Sm-A_d into the RN phase the smectic peaks disappear as expected. On further decreasing the temperature into the $\tilde{C}$ phase we did not observe along q_z any Bragg peak of the 2D monoclinic lattice. Evidently, in the $\tilde{C}$ grains the planes of the 2D ordering deviate from the direction parallel to the substrate. Upon rocking the film the accessible angular range ($\theta < 1°$ as restricted by the substrate) was too limited to see the scattering from these planes.

More insight is provided by XR and AFM of thin spin-coated films. Figure 2 depicts reflectivity data taken for the same material ($P_w = 55$) at various temperatures. The FWHM of a transverse scan across the specular reflectivity is typically 0.025°. The reflectivity curves show oscillations (Kiessig fringes) due to interference of the reflections from each of the two interfaces, which gives a film thickness of about 28 nm. A second-order Bragg peak at $q_z \approx 3.7$ nm^{-1} in both the Sm-A_d and the high-temperature nematic phase reveals smectic layering parallel to the interfaces with a periodicity of ~ 3.5 nm (equal to bulk Sm-A_d). The first-order Bragg peak is not detectable at the intensity level of the Kiessig fringes. The Bragg reflection disappears below $\sim 80\,^\circ$C, which signifies the transition to the RN phase. At the transition to the $\tilde{C}$ phase ($T = 54\,^\circ$C) we gradually lose the thickness oscillations starting from large $q_z$values, which is indicative of large-size irregular height corrugations at the free surface. After heating back to the RN phase and further to the Sm-A_d phase both the Kiessig fringes and the Bragg peak reappear (see Fig. 2). Hence the structure changes are reversible. However, after prolonged (> 6 h) annealing in the $\tilde{C}$ phase the Kiessig fringes do not reappear anymore upon subsequent heating. Evidently, irreversible changes have occurred that correspond to dewetting of the film induced by growing 2D $\tilde{C}$ domains (see below).

Using AFM we can reveal the changes in the surface topography corresponding to the XR results (see Fig. 3). The initial film (quenched after prolonged annealing at 105 °C in the Sm-A_d phase) shows extended terraces of an average height of 3.5–4 nm and a roughness of 0.3–0.5 nm. This observation indicates Sm-A_d layers oriented parallel to the free surface. After annealing in the RN or

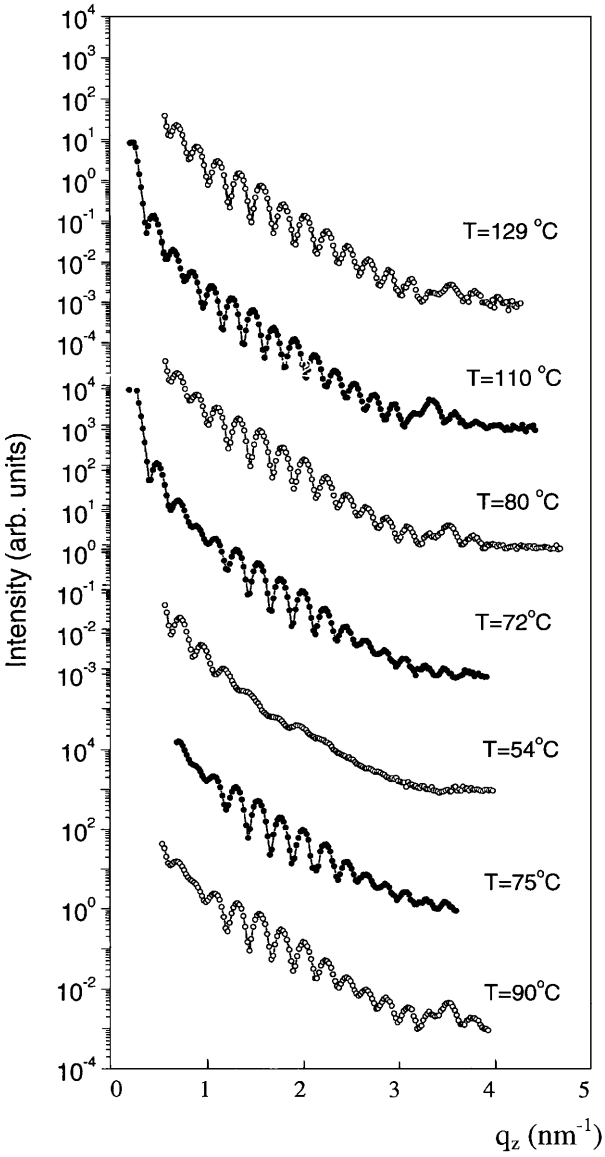

Fig. 2. X-ray reflectivity of a 28 nm film with $P_w = 55$ as a function of q_z at the temperatures indicated. Curves have been shifted for clarity.

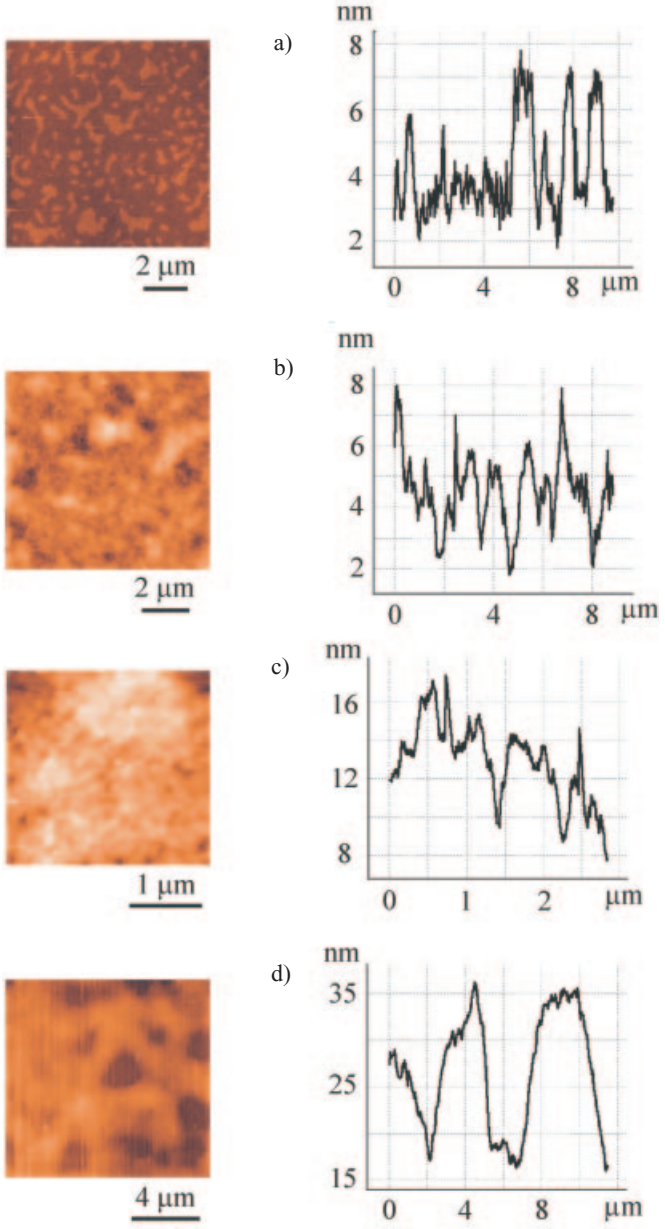

Fig. 3. AFM images for a 28 nm film with $P_w = 55$. (a) Annealed at $T = 105\,^{\circ}$C in the Sm-A_d phase (1.5×1.5 μm^2). The contrast corresponds to terraces with an average thickness of ~ 3.5 nm. (b) Annealed at $T = 75\,^{\circ}$C in the RN phase. (c, d) Annealed at $T = 53\,^{\circ}$C in the $\tilde{C}$ phase (different stages of dewetting are shown).

$\tilde{C}$ phase the surface roughness increases up to 0.8–1.5 nm and large-size holes start to develop with a thickness that exceeds the layer spacing. After prolonged annealing the depth of these holes (still with sharp edges) reaches the initial film thickness, which corresponds to dewetting of the film (see Fig. 3d). However, the surface topography of the remaining part of the film is still the same as before annealing.

A quite unusual surface topography has been revealed in thin films of PABB-5 with $P_w = 37$, which undergo a direct transition from the nematic to the $\tilde{C}$ phase. In Figure 4a the surface topography is shown after annealing in the nematic phase at $T = 85\,^{\circ}$C. We observe an extensive network of elongated asperities of an average height ~ 4.5 nm covering the film surface. XR from the same film (Fig. 4b) shows a broad bump at $q_z \approx 3.5$ nm^{-1} with Kiessig fringes on top and also a deepening of interference minima at $q_z \approx 1.7$ nm^{-1}. These results are indicative of surface-induced layering at the air-film interface. Indeed, the best fit to reflectivity gives a uniform density distribution in the interior of the film and a density modulation with a period of about 4 nm for the two top layers (as shown in the inset). The reduced electron density of the top layers is due to averaging over regions of different thickness within the illuminated area. Interestingly, the thickness of the surface-induced layers matches with

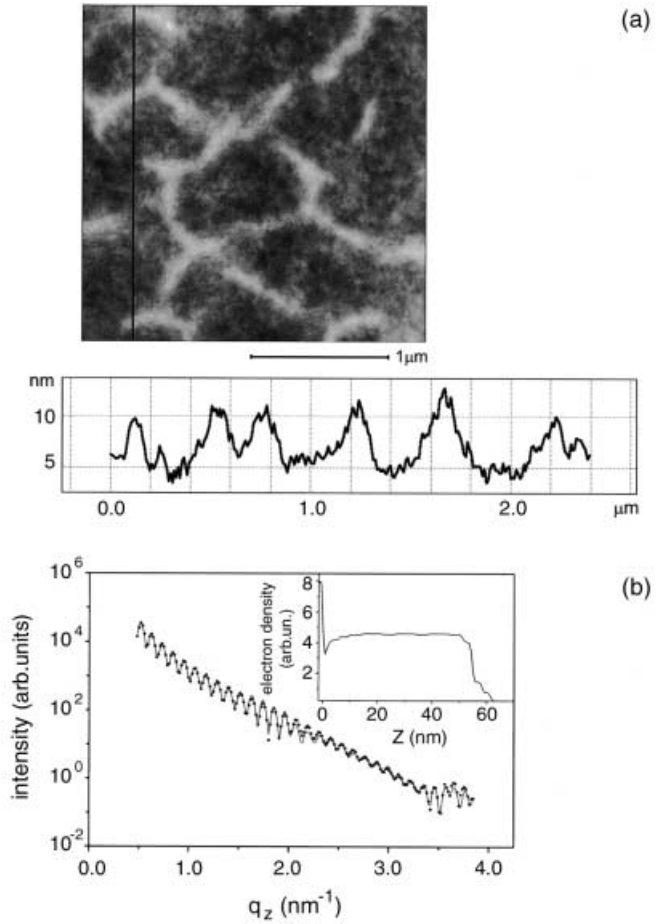

Fig. 4. (a) AFM topography ($2.5 \times 2.5\,\mu m^2$) of a 57 nm film with $P_w = 37$ annealed in the nematic phase at $T = 85\,^\circ C$ showing a 2D network of elongated asperities. The height profile (along the vertical line in the image) indicates an average thickness of the asperities of ~ 4.5 nm. (b) X-ray reflectivity of the same film. The solid line through the data points gives the best fit corresponding to the electron density profile in the inset. The broad bump at large q_z, decorated with interference fringes, indicates the presence of two surface layers with a thickness of about 4 nm.

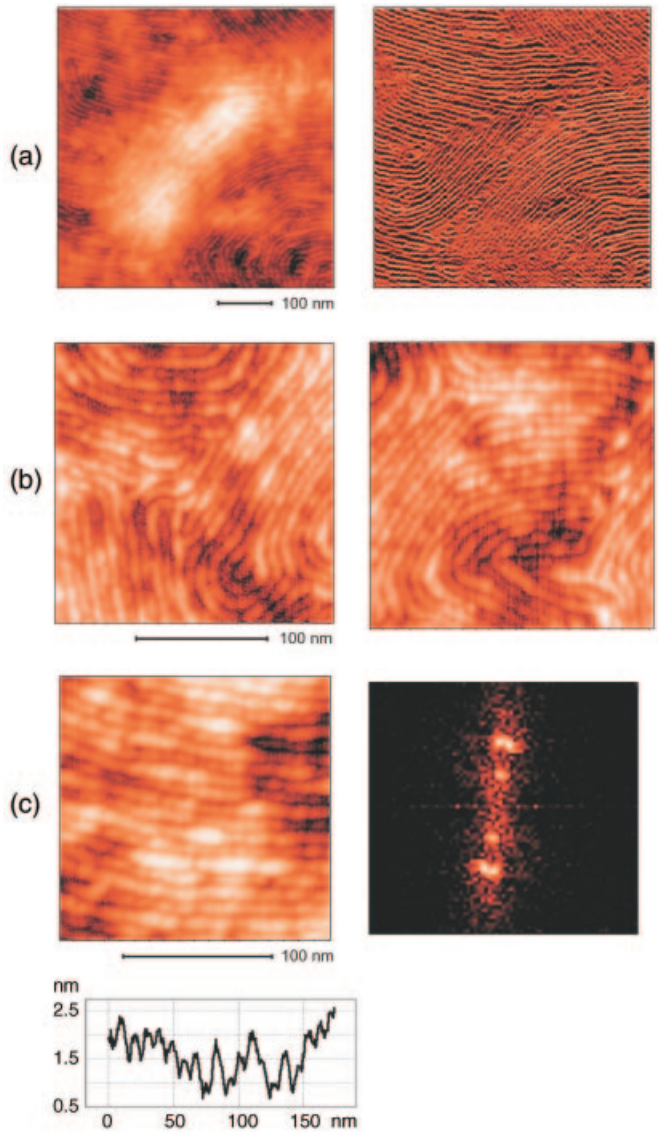

Fig. 5. Surface patterning in the film of Figure 4 as revealed by AFM at different magnification. (a) AFM topography ($0.5 \times 0.5\,\mu m^2$), showing surface ripples macroscopically oriented along an asperity, and phase image of the same area. (b) Typical defects in the molecular fingerprints ($0.22 \times 0.22\,\mu m^2$). (c) AFM topography ($0.18 \times 0.18\,\mu m^2$) and power spectrum of the surface modulations showing first- and second-order Bragg peaks. From the height modulation profile along the vertical line in the image, the average wavelength of the undulations is ~ 9 nm; the average height difference between two lamellae is 0.4–0.5 nm.

an *average* of the Sm-A_d spacing and the thickness of the $\tilde{C}$ bilayers, and the asperity height with the $\tilde{C}$ spacing. These findings corroborate the bulk measurements (see I) that show, for $P_w < 42$, strong $\tilde{C}$-type fluctuations in the nematic phase.

Zooming in on the same film reveals nanoscopic surface patterns over the whole surface (see Fig. 5). Well-defined lamellae with a lateral periodicity of about 9 nm are oriented along the direction of the elongated asperities (Fig. 5a). The height contrast is about 0.3–0.5 nm. Figure 5c displays a further magnification and a 2D fast Fourier transform of this image. Two orders of Bragg reflections indicate that the periodicity is long range. The surface patterns show locally line and point defects of the director field (Fig. 5b) similar to the boundaries of the cholesteric phase of liquid crystals [9,10]. Note a so-called $\lambda+$ defect in the left image. These surface patterns are not only present in the nematic phase for $P_w = 37$ but also in any of the other LC states of PABB-5 including the Sm-A_d and the RN phase, indicating a material property rather than a phase property.

4 Discussion

First we want to discuss in some more detail the X-ray reflectivity results of Figure 2. XR is determined by the electron density distribution along the film normal, averaged over the surface area over which the X-rays scatter coherently. Information regarding $\rho(z)$ and the interface roughness can be extracted by fitting the data to an iterative matrix solution of the Fresnel equations for the reflectivity of a multilayer system, convoluted with the instrumental resolution [11]. The film is described by a succession of homogeneous slabs, each characterized by three parameters: thickness, electron density and a Gaussian interfacial roughness σ. The electron density is related to the refractive index $n = 1 - \delta$ via $\rho = 2\pi\delta/(\lambda^2 r_e)$, where r_e is the classic radius of electron and δ is the so-called reduced density. In Figure 6a an initial best fit to the second reflectivity curve of Figure 2 is displayed (film in the Sm-A_d phase at $T = 110\,^\circ$C). Layers are represented by cells of ~ 3.5 nm smeared with an interfacial roughness of about 0.4–0.5 nm. Though this model well reproduces the general features of the reflectivity curve over a wide angular range, there are deviations from the experimental data in the vicinity of the second-order Bragg peak ($q_z \approx 3.7$ nm^{-1}). The fit can be improved upon by including the effects of the boundaries on the smectic density wave. This can be done by assuming that the amplitude $\Delta\rho$ of the density modulation depends on the distance from both interfaces. To introduce this effect, the variation of the density ρ_m of the m-th layer (unit cell, $m = 1$ is the top layer) with m expressed in the form

$$\rho_m = \langle\rho\rangle + \Delta\rho \exp\left[A(m-1) - B(m-1)^2\right], \quad (1)$$

in which $\langle\rho\rangle$ is the average density, $\Delta\rho = \rho_1 - \langle\rho\rangle$ and A and B are adjustable parameters. Equation (1) describes the simplest form of nonlinear exponential decay, which provides the suggested boundary effects. To introduce the smectic layer form factor the unit cell was divided into two sub-layers of different electron density and thickness. The denser area corresponds to the overlapping regions of the mesogenic cores, while the aliphatic tails and backbone fragments contribute to the less dense region. The electron density distribution across the film can be divided into three regions: the part adjacent to the substrate, the periodic middle part and the part near the free surface. Figure 6b shows the resulting best fit to the XR data using the parameters given in Table 1, highlighted around the second-order Bragg peak. Figure 6c illustrates the resulting density profile according to equation (1), which indicates that the smectic lamellae are better developed at the interfaces than in the middle of the film. The optimised model consists of a layer adjacent to the substrate of about 2.8 nm, seven smectic layers with a spacing $d = 3.5 \pm 0.1$ nm determined by the sum of two sub-layers, and a top layer of about 2.2 nm with a reduced density at the film-air interface. The latter effect is directly visible in AFM, which indicates terraces in the top layer over which XR averages laterally [12].

From the XR and AFM studies of thin films of the PABB-5 polyacrylate, we conclude that lamellar ordering parallel to the surface is supported close to the film-air and film-substrate interfaces. However, the density modulation decays with increasing distance from the interfaces. This observation is in agreement with the absence of Bragg peaks in thick Sm-A_d films of PABB-5

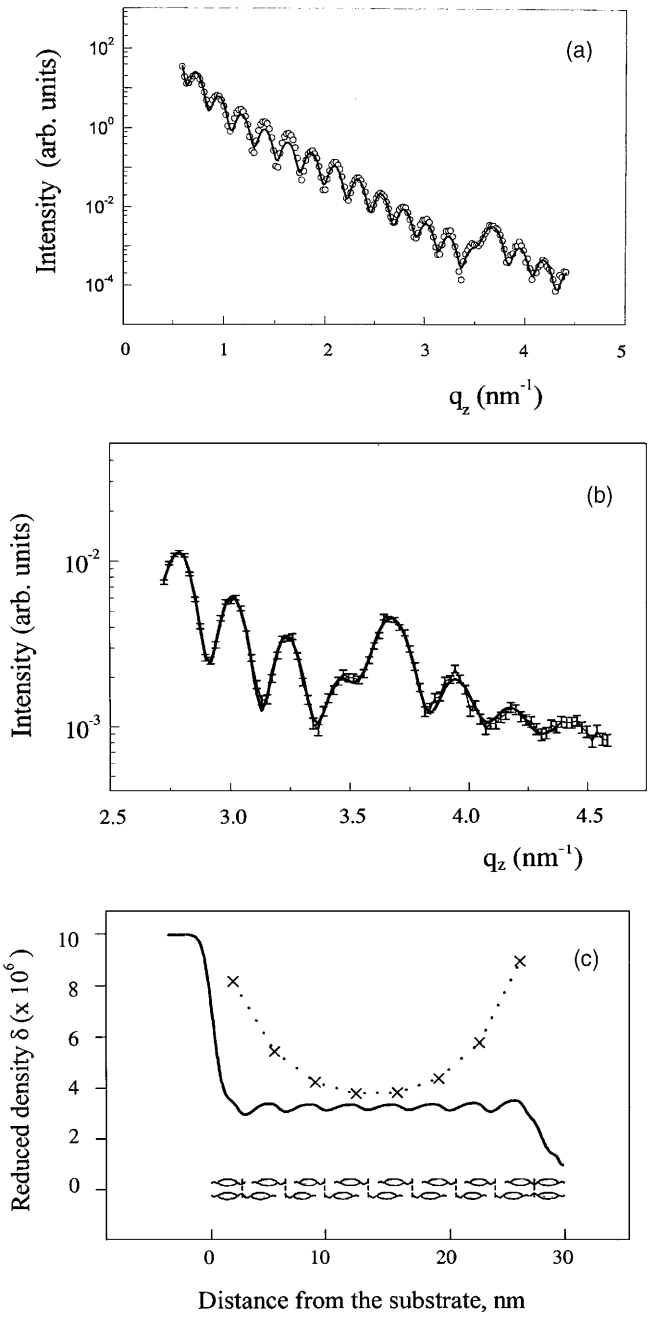

Fig. 6. X-ray reflectivity of a 28 nm film with $P_w = 55$ in the Sm-A_d phase at $T = 110\,^\circ$C. (a) Initial fit with a constant amplitude of the smectic density modulation. (b) Improved fit with variable amplitude, illustrated around the second Bragg peak. (c) Model electron density across the film (solid line) together with the amplitude of the density modulation over the layers (crosses). The value of $\Delta\rho$ in equation (1) in the middle of the film is about 40% of that of the top layer.

Table 1. Film parameters corresponding to the XR fitting according to equation (1) as shown in Figure 6b. The error bars correspond to 95% confidence limit. The constants in equation (1) have the values $A = -0.56 \pm 0.2$ and $B = (-8.2 \pm 2.4) \times 10^{-2}$.

	δ ($\times 10^6$)	d (nm)	σ (nm)
Substrate	10	–	0.89 ± 0.05
Layer adjacent to substrate	3.5 ± 0.8	2.78 ± 0.1	0.58 ± 0.09
1st sub-layer core (7×)	3.6 ± 0.9	2.10 ± 0.01	0.46 ± 0.06
2nd sub-layer core (7×)	3.0 ± 0.8	1.37 ± 0.09	0.73 ± 0.23
Averaged top layer	1.6 ± 0.3	2.17 ± 0.05	0.24 ± 0.08

(compare Fig. 1, open squares). Homeotropic anchoring at an air-film surface (leading to smectic layering parallel to the interface) has been reported to be quite general for LC polymers with aliphatic chain-terminated side groups [13,14]. However, this behaviour was primarily established for LC polymers with methacrylate and siloxane backbones. For a polyacrylate like PABB-5 the experimental situation is more delicate: the mesogenic side chains indeed show homeotropic anchoring at the film interfaces, but this ordering does not penetrate strongly into the interior. It seems that for the present polyacrylates the interior side groups do not adjust to the homeotropic anchoring at the interface, due to the coupling with the randomly distributed backbone. This prevents the smectic layering parallel to the interface from developing into the film interior. According to the thick-film results of Figure 1, this situation changes dramatically in a narrow temperature range near the Sm-A_d–RN phase transition, where an ordering transformation takes place: the smectic layers become parallel to the surface in the whole film (Fig. 1, filled dots). We speculate that a change from an oblate to a prolate backbone conformation, which according to I occurs in the same temperature range, triggers this ordering transformation. This interpretation is supported by the reversibility of the transformation upon cycling the temperature. Due to the large viscosity of the polymer the complete smectic layer rearrangement takes in the thick films about 2-3 hours. Such an ordering transformation has not been observed in the thin films. Most probably the strong confinement in this situation leads to a strong increase of the corresponding transformation time.

For $P_w = 37$ we conclude from Figures 4 and 5 that $\tilde{C}$-type bilayers start to grow in the nematic phase from the surface in the form of a 2D network of asperities. With decreasing temperature the Kiessig fringes in the reflectivity from the film disappear starting from large q_z values, similar as observed for $P_w = 55$ (Fig. 2). They disappear completely at temperatures corresponding to the region of stability of the $\tilde{C}$ phase. From AFM again a clear picture of polymer dewetting evolves. With decreasing temperature the dewetting proceeds via an increasing average roughness at the free surface, in combination with the formation of top bilayers in the form of elongated islands. At a certain stage the large-size holes become larger than the layer spacing, and after prolonged annealing reach the thickness of the initial film. From this point of view the formation of a 2D network of asperities in the nematic phase might be considered as the initial stage of structural dewetting in the film. To explain dewetting of thin liquid and LC films on solid substrates, two different mechanisms have been proposed [15]: 1) nucleation at defects and subsequent growth, 2) amplification of thermal fluctuations at the free surface leading to so-called spinodal dewetting. However, also different examples exist in which a restructuring of the molecules at the substrate or in the interior of the film destabilizes the free surface of a film [16]. This can result in the development of holes at the free surface that may lead to a dewetting behaviour resembling spinodal dewetting. We speculate that in the case of the present LC polyacrylates the creation of holes and dewetting of polymer films is due to the growth of 2D $\tilde{C}$-like surface domains.

Spinodal-like dewetting in liquid as well as polymer films has been reported to produce surface undulations with periodicities on the scale of microns [15,16], in contrast to the nanometer scale of the surface lamellae presented here. Similar height modulations have also been observed at the surface of cholesteric oligomers in their glassy state [9], though at a much larger length scale (about 200 nm). The characteristics of the surface ripples in a PABB-5 film resemble those of the ripple phase of lipid membranes [17]. Such membranes consist of bilayers of amphiphilic molecules with their hydrocarbon tails shielded from the surrounding water. They are flexible and may form phases with a periodic surface corrugation on the scale of 10–20 nm. Surface ripples in a soft matter film generally can arise due to a subtle coupling between surface curvature and some local internal variable, which may be as different as hydrocarbon chain conformation, tilt angle or local composition [18,19]. In the present LC polymers the local order can be described in a natural way by an order parameter giving the degree of overlap of the mesogenic side chains. The lamellar thickness at the surface may vary locally because of the existence of two stable side-chain packing configurations with spacings of 3.5 and 4.4 nm (see Fig. 7). The amplitude of the surface ripples ($\sim$ 0.4–0.5 nm) corresponds to half the difference of these two spacings. Hence the surface ripples may originate from a frustration of the surface-induced layering, the competition between the two possible periodicities at the surface being accommodated by film curvature. The amplitude is relatively small compared to the top layer thickness, which makes the surface ripples behave as undulations of the lamellar thickness. A similar effect might

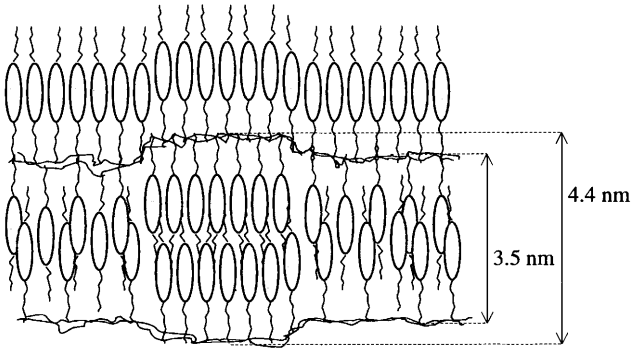

Fig. 7. Sketch of the two types of mesogenic spacings contributing to the top layer undulations.

exist also at the free interface of low molecular mass frustrated mesogens. For example, bilayers have been observed at the free surface of a terminally polar mesogen with a single layer bulk structure [20]. The surface topography of such materials has not been studied so far.

The nanoscale surface patterning can be qualitatively described by extending the phenomenological model of Leibler and Andelman [18]. This model attributes the formation of ordered mesostructures in membranes and amphiphilic films to a coupling between the curvature of the film and a local internal variable. In PABB-5 competition exists between two layer spacings, corresponding to different degrees of overlap of the side chains. Hence an appropriate choice of a scalar order parameter is $\phi = d - d_0$, where d_0 is a reference layer periodicity taken here as that of the Sm-A_d phase. The corresponding Hamiltonian for the displacement $w(\mathbf{r}_\perp = x, y)$ of the film relative to a flat reference plane, can be written as

$$H = \frac{1}{2}\int \mathrm{d}\mathbf{r}_\perp \Big[\gamma\left(\nabla_\perp w\right)^2 + K\left(\nabla_\perp^2 w\right)^2 + f(\phi) + c\left(\nabla_\perp \phi\right)^2 + 2\lambda\phi\left(\nabla_\perp^2 w\right)\Big],$$

$$f(\phi) = a\phi^2 + \frac{1}{2}b\phi^4 . \qquad (2)$$

Here γ is the surface tension, K is the layer bending modulus and a, b, c and λ are phenomenological coefficients. The first two terms in equation (2) represent the contributions of the surface and of the bending, respectively. The term $f(\phi)$ is the Landau expansion of the free-energy density around the critical point $d = d_0$. The first gradient term describes the spatially nonuniform fluctuations of the scalar field ϕ, the coefficient c being a measure of the "strength" of the fluctuations. The last term corresponds to the lowest-order coupling between ϕ and the lamellar curvature. Without the gradient terms, equation (2) gives the usual critical point at $a = 0$. Equation (2) can be expressed in momentum space as [18]

$$H = \frac{1}{2}\int \mathrm{d}\mathbf{q}_\perp \left[q_\perp^2\left(c - \lambda^2/\gamma\right)\phi_q^2 + q_\perp^4\left(\lambda^2 K/\gamma^2\right)\phi_q^2\right] + \int \mathrm{d}\mathbf{r}_\perp f(\phi) . \qquad (3)$$

The form of equation (3) is widely used to describe the critical behaviour in the vicinity of a so-called Lifshitz point, where the coefficient $(c - \lambda^2/\gamma)$ of the $q_\perp^2$-term and a in $f(\phi)$ are simultaneously equal to zero [21]. If $(c - \lambda^2/\gamma) > 0$, the ordered phase will be spatially uniform. However, for $\lambda > \sqrt{c\gamma}$, this coefficient is negative and the homogeneous phase becomes unstable with respect to long-wavelength fluctuations. The system can decrease its energy by creating spatially modulated structures with a wave vector $q_0 = \gamma[(c - \lambda^2/\gamma)/(2\lambda^2 K)]^{1/2}$. An estimate of the undulation period $2\pi/q_0$ using typical LC polymer parameters leads to a value of the order of 10–100 nm, qualitatively in agreement with the picture of Figure 5. The formation of modulated structures can also be described as a system of defect walls separating areas of different spacings in the surface layers [21].

In conclusion, we have investigated films of PABB-5, a new type of frustrated side-chain liquid crystalline polymer described in part I (preceding paper). In the system two stable side-chain packing configurations with incommensurate spacings exist. The free surface in thin polymer films can stabilise surface layers of these competing periodicities. Depending on the degree of polymerisation, thin films in the nematic phase show a structural dewetting induced by the growth of surface $\tilde{\mathrm{C}}$-like domains. Furthermore, the coupling between the local liquid crystalline ordering of the side groups and the surface curvature induces ripples at the air-film interface with a nanometer-scale lateral period. These modulations can be understood phenomenologically in analogy with surface ripples in membranes. These self-organizing properties of PABB-5 provide an easy way to pattern a homogeneous surface laterally.

The authors wish to thank A.R. Khokhlov and B. Mulder for valuable discussions. This work is part of the research program of the "Stichting voor Fundamenteel Onderzoek der Materie, (FOM)", which is financially supported by the "Nederlandse Organisatie voor Wetenschappelijk Onderzoek, (NWO)". BIO acknowledges support from NWO in the framework of the cooperation program with the Russian Federation. We also acknowledge support from Russian Fund for Fundamental Research (under grant 00-03-33174).

References

1. B.I. Ostrovskii, S.N. Sulyanov, N.I. Boiko, V.P. Shibaev, W.H. de Jeu, this issue, p. 277.
2. A preliminary account has been given in D. Sentenac, B.I. Ostrovskii, W.H. de Jeu, Adv. Mater. **13**, 1079 (2001).
3. Y. Xia, J.A. Rogers, K.E. Paul, G. Whitesides, Chem. Rev. **99**, 1823 (1999).
4. E. Schäffer, T. Thurn-Albrecht, T.P. Russell, U. Steiner, Nature **403**, 874 (2000); T.L. Morkved, M. Lu, A.M. Urbas, E. Ehrichs, H.M. Jaeger, P. Mansky, T.P. Russell, Science **273**, 931 (1996).
5. L. Rockford, Y. Liu, P. Mansky, T.P. Russell, M. Yoon, S.G.J. Mochrie, Phys. Rev. Lett. **82**, 2602 (1999); A.M. Higgins, R.A.L. Jones, Nature **404**, 476 (2000); P. Mansky,

Y. Liu, E. Huang, T.P. Russell, C.J. Hawker, Science **275**, 1458 (1997).
6. M. Park, C. Harrison, P.M. Chaikin, R.A. Register, D.H. Adamson, Science **276**, 1401 (1997); T. Thurn-Albrecht, R. Steiner, J. DeRouchey, C. Stafford, E. Huang, M. Bal, M. Tuominen, C.J. Hawker, T.P. Russell, Adv. Mater. **12**, 787 (2000).
7. N.I. Boiko, V.P. Shibaev, B.I. Ostrovskii, S.N. Sulyanov, D. Wulff, J. Springer, Macromol. Chem. Phys. **202**, 297 (2001).
8. S. Gierlotka, P. Lambooy, W.H. de Jeu, Europhys. Lett. **12**, 341 (1990); E.A.L. Mol, J.D. Shindler, A.N. Shalaginov, W.H. de Jeu, Phys. Rev. E **54**, 536 (1996).
9. R. Meister, H. Dumoulin, M.-A. Halle, P. Pieranski, J. Phys. II **6**, 827 (1996); R. Meister, M.-A. Halle, H. Dumoulin, P. Pieranski, Phys. Rev. E., **54**, 3771 (1996).
10. P.G. de Gennes, J. Prost, *Physics of Liquid Crystals*, 2nd edition (Clarendon Press, Oxford, 1992) p. 316.
11. I.I. Samoilenko, O.V. Konovalov, L.A. Feigin, B.M. Shchedrin, L.G. Yanusova, Cryst. Rep. **44**, 347 (1999).
12. See, for example, G. Reiter, *X-ray and Neutron Reflectivity: Principles and Applications*, edited by J. Daillant, A. Gibaud (Springer, Berlin, Heidelberg, 2000) p. 305 and references therein; D. Sentenac, A.L. Demirel, J. Lub, W.H. de Jeu, Macromolecules **32**, 3235 (1999).
13. B. Jerome, J. Commandeur, W.H. de Jeu, Liq. Cryst. **22**, 685 (1997) and references therein.
14. H. Mensinger, M. Stamm, C. Boffel, J. Chem. Phys. **96**, 3183 (1992); H. Elben, G. Strobl, Macromolecules **26**, 1013 (1993); I. Entin, R. Coffer, D. Davidov, I. Hersht, Phys. Rev. B **47**, 8265 (1993); G. Decher *et al.*, Ber. Bunsenges. Phys. Chem. **97**, 1386 (1993); G.C.L. Wong, J. Commander, H. Fisher, W.H. de Jeu, Phys. Rev. Lett. **77**, 5221 (1996).
15. See, for example, S. Herminghaus, K. Jacobs, K. Mecke, J. Bishof, A. Fery, M. Ibn-Elhaj, S. Schlagowski, Science **282**, 916 (1998); G. Reiter, A. Sharma, R. Khanna, A. Casoli, M.-O. David, J. Colloid Interface Sci. **214**, 126 (1999) and references therein.
16. A.L. Demirel, B. Jerome, Europhys. Lett. **45**, 58 (1999) and references therein.
17. J.A. Zasadzinski, J. Schneir, J. Gurley, V. Elings, P.K. Hansma, Science, **239**, 1013 (1988); J.T. Woodward, J.A. Zasadzinski, Phys. Rev. E **53**, 3044 (1996).
18. S. Leibler, D. Andelman, J. Phys. **48**, 2013 (1987); R.E. Goldstein, S. Leibler, Phys. Rev. A **40**, 1025 (1989).
19. W. Scott McCullough, H. L. Scott, Phys. Rev. Lett. **65**, 931 (1990); C-M Chen, T. C. Lubensky, F. C. Mackintosh, Phys. Rev. E **51**, 504 (1995).
20. E.F. Gramsbergen, W.H. de Jeu, J. Als-Nielsen, J. Phys. **47**, 711 (1986).
21. See, for example, P.M. Chaikin, T.C. Lubensky, *Principles of Condensed Matter Physics* (Cambridge, 1995) Chapt. 4.